AIP | Review of Scientific Instruments

Temperature and density evolution during decay in a 2.45 GHz hydrogen electron cyclotron resonance plasma: Off-resonant and resonant cases

O. D. Cortázar, A. Megía-Macías, and A. Vizcaíno-de-Julián

Citation: Rev. Sci. Instrum. **84**, 093301 (2013); doi: 10.1063/1.4819875
View online: http://dx.doi.org/10.1063/1.4819875
View Table of Contents: http://rsi.aip.org/resource/1/RSINAK/v84/i9
Published by the AIP Publishing LLC.

Temperature and density evolution during decay in a 2.45 GHz hydrogen electron cyclotron resonance plasma: Off-resonant and resonant cases

O. D. Cortázar,[1,2,a)] A. Megía-Macías,[1] and A. Vizcaíno-de-Julián[1]
[1]*ESS Bilbao, Edificio Cosimet, Landabarri 2, 48940-Leioa, Vizcaya, Spain*
[2]*Universidad de Castilla-La Mancha, ETSII, C.J. Cela s/n, 13170 Ciudad Real, Spain*

(Received 24 April 2013; accepted 19 August 2013; published online 5 September 2013)

Time resolved electron temperature and density measurements during the decay stage in a hydrogen electron cyclotron resonance (ECR) plasma are presented for a resonance and off-resonance magnetic field configurations. The measurements are conducted on a ECR plasma generator excited at 2.45 GHz denominated test-bench for ion-sources plasma studies at ESS Bilbao. The plasma parameters evolution is studied by Langmuir probe diagnostic with synchronized sample technique developed for repetitive pulsed plasmas with a temporal resolution of 200 ns in typical decay processes of about 40 μs. An afterglow transient is clearly observed in the reflected microwave power signal from the plasma. Simultaneously, the electron temperature evolution shows rebounding peaks that may be related to the interplay between density drop and microwave coupling with deep impact on the Electron Energy Distribution Function. The correlation of such structures with the plasma absorbed power and the coupling quality is also reported. © *2013 AIP Publishing LLC*. [http://dx.doi.org/10.1063/1.4819875]

I. INTRODUCTION

The study of physical processes during the decay in pulsed Electron Cyclotron Resonance (ECR) plasmas is of extended interest in the Electron Cyclotron Resonance Ion Source (ECRIS) community. Since the afterglow effect was reported by Melin *et al.*[1] in 1990, an intensive research activity has been developed in order to understand such transient effect,[2–5] and a recent contribution on the basis of time resolve bremsstrahlung diagnostics has shown the influence of cyclotron instabilities.[6] On the other hand, studies at ESS Bilbao ECR plasma project have been focused on time-resolved diagnostics during breakdown process.[7–10] Such experience is exploited in this paper where we present a study of the decay in our 2.45 GHz ECR hydrogen plasma generator denominated T.I.P.S. (Test-bench for Ion-sources Plasma Studies) for resonance and off-resonance magnetic field profiles at different powers and hydrogen pressures. We combine the measurements of incoming and reflected microwave power with time resolved electron temperature and density by means of Langmuir probe diagnostics. An afterglow transient is clearly observed in the reflected power signal records with a corresponding structure of rebounding peaks in the electron temperature evolution.

II. PLASMA GENERATOR

A detailed description of the system can be found in Refs. 7 and 10. A plasma generator driven by a 3 kW adjustable power magnetron of 2.45 GHz operated at 100 Hz in pulsed mode is used. Figure 1 shows a cross section view of reactor. A diagnostic port (a) with pumping and probe (b) is attached to the cylindrical plasma chamber (c) made of oxygen-free high thermal conductivity (OFHC) copper with 93 mm length by 90 mm diameter. A set of four coaxial coils arranged in two pancakes (d) with independently adjustable currents and a positioning mechanism produce different magnetic field profiles. Hydrogen flows into the chamber through the inlet port (e), while a 10 mm thickness quartz window (f) separates the vacuum enclosure from the microwave driver system. A ridged waveguide coupler (g) is used for adapting impedances of plasma chamber and WR330 model microwave waveguide. Pressure values inside the plasma chamber are measured by a penning type gauge connected to the gas pressure inlet (h). A two-stub tuner is used for fine impedance matching and bidirectional couplers give readings of incoming and reflected power from magnetron and plasma, respectively (both not visible in Fig. 1).

III. MAGNETIC FIELD PROFILES

Two magnetic field configurations have been used during the experiments to study its influence on the decay process. The choice of such configurations responds to "off-resonance" and "resonance" cases where a good plasma stability behavior has been found allowing to set a reliable experimental arrangement as is described in Sec. IV. Figure 2 shows both Bz magnetic field profiles along the z-axis experimentally measured by a vector magnetic probe with a typical error of ± 1 mT. Note that longitudinal plasma chamber limits are indicated by dotted vertical lines, where the left one shows the microwave injection side and the right one the diagnostics side. The ECR magnetic field level of 87.5 mT is marked with a dashed flat line. Curve (a) shows the off-resonance case of longitudinal asymmetric field distribution with a maximum value of 130 mT in the proximities of the diagnostic port, and 120 mT in the middle of the chamber. Curve (b) shows the resonance case with a symmetrical distribution around of ECR value. Figure 3 shows a 2D magnetic map simulation

a)Electronic mail: dcortazar@essbilbao.org

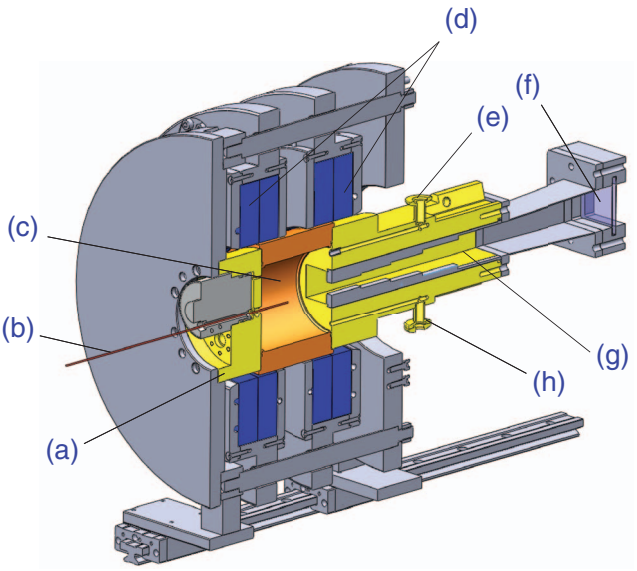

FIG. 1. Cross section view of the plasma generator: (a) Diagnostic port, (b) Langmuir probe, (c) plasma chamber, (d) coils pancakes, (e) gas inlet, (f) quartz window, (g) ridge microwave coupler, and (h) pressure gauge inlet.

for each case of study where half chamber is represented in full black line and the low border is coincident with z-axis. Magnetic map (a) represents the off-resonance case where B > ECR, and (b) the resonance case where B ≃ ECR in most of chamber volume. It is clear that both cases are corresponding to curves (a) and (b) of Fig. 2, respectively. Dashed black lines indicate the ECR surface positions separating the volumes where magnetic field is lower and higher with respect to ECR value. These simulations have been validated by magnetic probe direct measurements in the plasma chamber volume. Note that both field topologies are not magnetic mirrors because this plasma generator has been originally designed with the purpose to study hydrogen plasmas for proton generation without trapping to enhance confinement time in order to reach high ionization degrees.

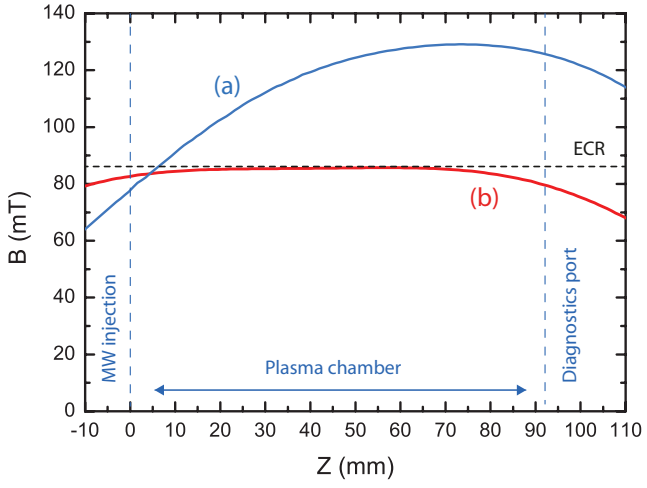

FIG. 2. Z axial magnetic profiles used during experiments. (a) Off-resonance asymmetric Bz > ECR, and (b) resonance symmetric Bz ≃ ECR magnetic profile.

IV. TIME RESOLVED PROBE DIAGNOSTICS

Langmuir probes are usually used embedded in plasmas for acquiring characteristic I-V curves, which permit to estimate plasma electron temperature and density. Time resolved measurements made on several kinds of plasma generators have been conducted recently for repetitive pulsed operation during plasma transients.[3,5,7,8,11] In general terms, these measurements have been obtained taking the I-V curve points one by one from different consecutive pulses completing the voltage sweep in a predetermined time. When synchronization is carefully made, keeping the jitter low enough during the process, it is possible to obtain an estimation of electron density and temperature at a precise predefined instant. Figure 4 shows a conceptual scheme where this technique is represented from a typical I-V curve and an oscilloscope record, both obtained in the experiment. In our case the system acquires an I-V point during 62.5 ns, and after approximately 14.6 μs (time necessary for digitalizing and storing data) it is ready to take the next one. This process is averaged twenty times before moving to the next I-V point. Applying this method, time resolved I-V curves can be obtained by synchronizing Langmuir probe trigger driver and magnetron via a delay generator. Several pulses can be seen in the oscilloscope record of Fig. 4 where signals (a) are the incoming power, (b) are the reflected power, and (c) are the synchronism pulses from probe driver system. Note that amplifications for both (a) and (b) channels are the same. In order to see more precisely the instant where data are collected, it is necessary to zoom the decay stage interval of time. An example of a typical timing record during the study of the decay transient is shown in Fig. 5 where signal (a) is the incoming power, (b) is the reflected power, and (c) is the synchronism pulse from probe driver system. The front of this pulse represents the instant where measuring is taking place. Note that in this case, signal (b) is ten times amplified with respect to signal (a). This is because the reflected power is low during the pulse body, and it is necessary to increase the amplification in order to see the structure of the plasma power emission, once the microwave incoming power is off. Figure 6 shows the experimental set-up where the timing strategy is shown. Note, how the delay pulse generator produces a predetermined synchronization by firing the probe driver system with a Transistor-Transistor Logic pulse. A sample of such signal is recorded in the oscilloscope in order to check the instant of time where I-V curve is obtained as shown in Fig. 5(c).

Initially, tungsten wire probes of 0.05 and 0.1 mm diameter by 6 mm long were used following the criteria design of Chen[12] for RF argon low density plasmas, but low intensity and noisy curves were obtained. After increasing the probe diameter to 0.5 mm, reliable results with a remarkable reproducibility have been measured in our hydrogen plasma by placing the probe tip in the middle of plasma chamber (r = 0 and z = 46 mm). The Langmuir probe driver consists on ESPION system made by Hiden Analytical LTD. Jitter is carefully checked obtaining a value lower than 200 ns in order to ensure measurement quality. By modifying Langmuir probe trigger delay, a set of I-V curves during the plasma decay has been obtained.

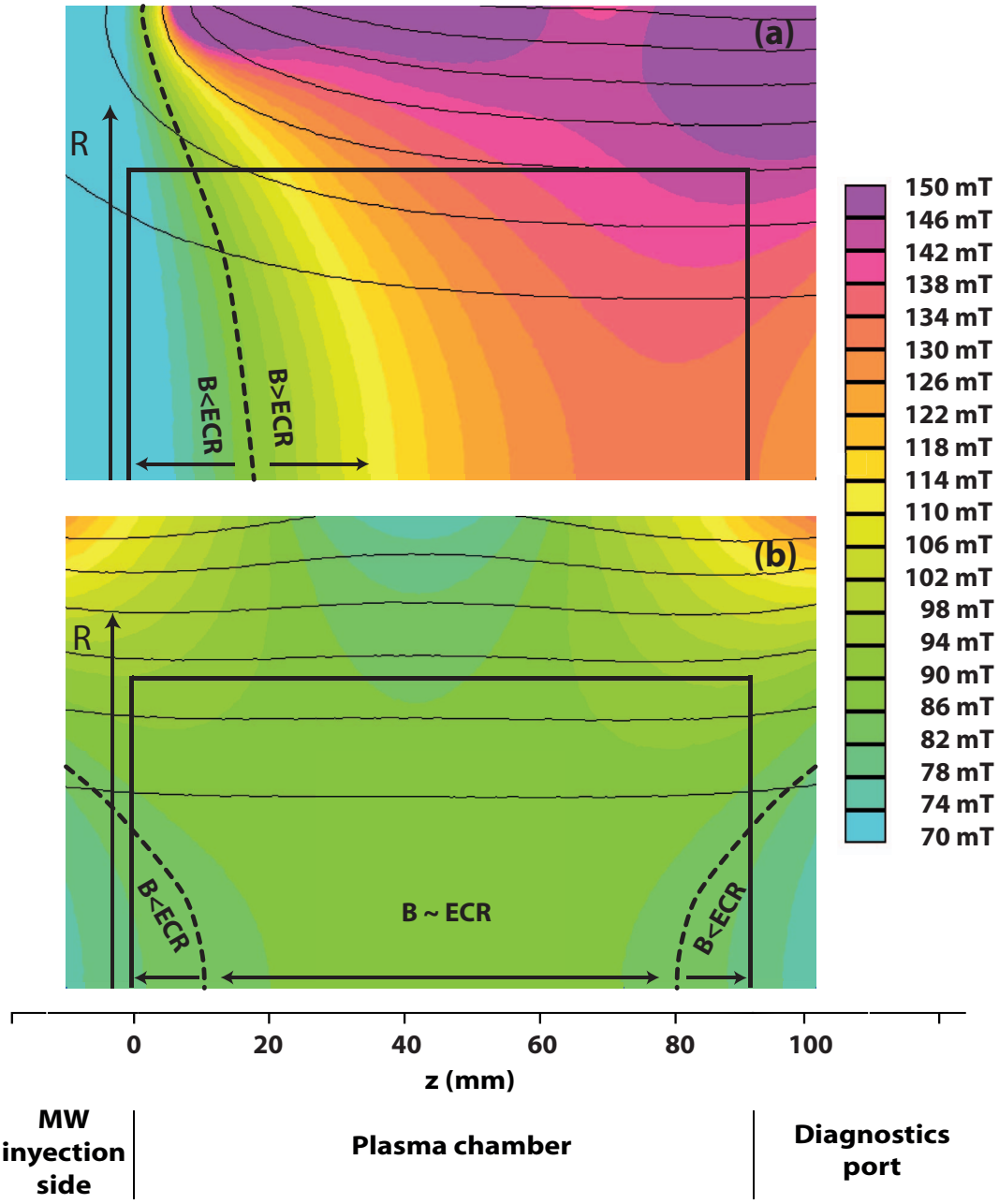

FIG. 3. 2D revolution view of magnetic field profiles used during the experiments obtained by simulation. Only half chamber is represented where the low border is coincident with the z-axis. Black solid line represents the plasma chamber volume. Profile (a) is the off-resonance case where B > ECR, and (b) is the resonance case where B $\simeq$ ECR in most of the plasma chamber volume. Dashed black lines represent the position of ECR surfaces.

V. DATA ANALYSIS AND CALCULATIONS

Typical I-V curves as obtained during experiments are shown in Fig. 7. Case (a) is a curve obtained 100 μs before incoming microwave pulse is off where the plasma can be considered in steady-state, and case (b) is a curve obtained during the decay transient. Note that current intensities recorded in case (b) are more noisy and ten times lower than in case (a) according to density drop during decay. Due to this fact, we have paid special attention to calculations made with this kind of data focusing our efforts on these curves evolution during decay process starting from the steady-state situation.

In general terms, for both cases, the ion current increases following negative voltage without showing ion current saturation being effect remarkable for the decay transient. For low plasma densities and small probes, the sheath expansion effect produces an increase in the collected current because effective area for particle collection is the sheath area and not the geometric probe area.[13,14] Such situation is reflected by ion currents that do not show clear saturation values increasing gradually with increasing negative voltage. The slope in the I-V curve ion current branch is an unequivocal sign of low density plasma always with values under critical density of 7.44×10^{16} m^{-3} for 2.45 GHz microwaves. On the other

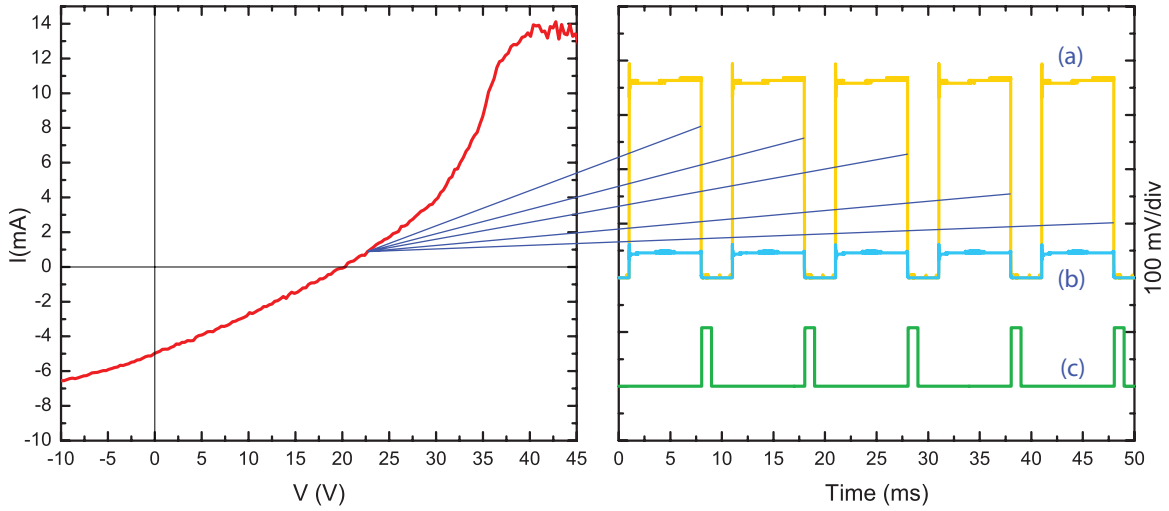

FIG. 4. Conceptual scheme showing that each point of the I-V curve (left) is obtained by averaging 20 measurements obtained in different consecutive pulses (right). Note that signal (a) is the incoming power, (b) the reflected power, and (c) are the synchronism pulses to check proper timing.

hand, the electron temperature T_e is generally estimated from I-V curves assuming a Maxwellian Electron Energy Distribution Function (EEDF) even when it is well known that such assumption can not be supported during transient stages like breakdown or decay of pulsed plasmas. In this way, the development of methods to calculate the EEDF and plasma parameters from experimental probe data during plasma transients with non-Maxwellian EEDFs is still a matter of open research and discussion.[15,16] In this work, temperatures and densities calculations are made by two different methods that are explained in Subsections V A and V B and that we have used in previous studies of breakdown processes.[7,9,10]

A. Difference of plasma and floating potentials

This method estimates the plasma temperature by using the difference of plasma and floating potentials. Two expressions are well known for these calculations, the one proposed for Lieberman and Lichtemberg in the book,[17]

$$V_p - V_f = kT_e \ln\sqrt{(m_i/2\pi m_e)}, \tag{1}$$

and the practically equivalent proposed by Saudit and Chen,[18]

$$V_p - V_f = (kT_e/2)\ln(2m_i/\pi m_e), \tag{2}$$

where V_p is the plasma potential, V_f is the floating potential, kT_e is in units of eV, m_i is the unit mass of the ion, and m_e is the unit mass of the electron. For hydrogen plasmas with varying species, fractions of Eqs. (1) and (2) take the form $T_e = 0.26...0.35(V_p - V_f)$. We have used a coefficient of 0.35 due to the external magnetic field that may increase the coefficient to values >0.3.[19] Obviously, for using this method, it is necessary to determine V_f and V_p from the experimental I-V curve. V_f is determined as the I-V curve zero crossing, and V_p as the maximum value of the first I-V derivative reaching to an estimation of the temperature value $T_{e,1}$. On the other hand, electron density is calculated by

$$n_e = \frac{4I_{es}}{eA_p\sqrt{8kT_e/\pi m_e}}, \tag{3}$$

where I_{es} is the electron saturation current, e is the electron unit charge, and A_p is the surface of the cylindrical probe. It is clear that for using Eq. (3), it is necessary to estimate I_{es}. Considering that at V_p the measured current is the sum of I_{es} and the ion current value at this point, I_{es} can be estimated. This estimation has to be made assuming some approximations on the ion current. In other words, we have to fit the behavior of the ion current in the left branch of the I-V curve to estimate I_{es}. If the fitting employed is linear, then I_{es} is calculated as the difference between the current measured at the plasma potential $I(V_p)$ and the value obtained with the linear fitting at the same voltage V_p.[13] However, if the fitting employed is parabolic according to Laframboise's calculations,[14,20] the value of the ion current at the plasma

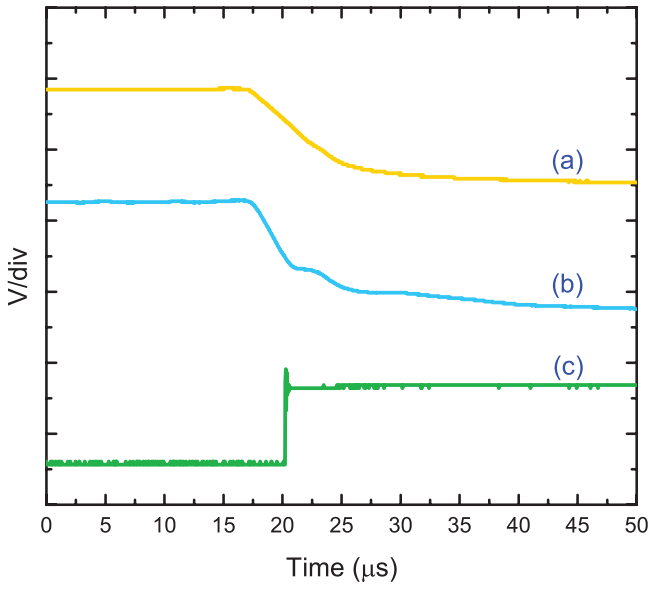

FIG. 5. View of a synchronism record during decay process: (a) is the incoming power, (b) is the reflected power, and (c) is the synchronism pulse where its rise indicates the instant of measuring.

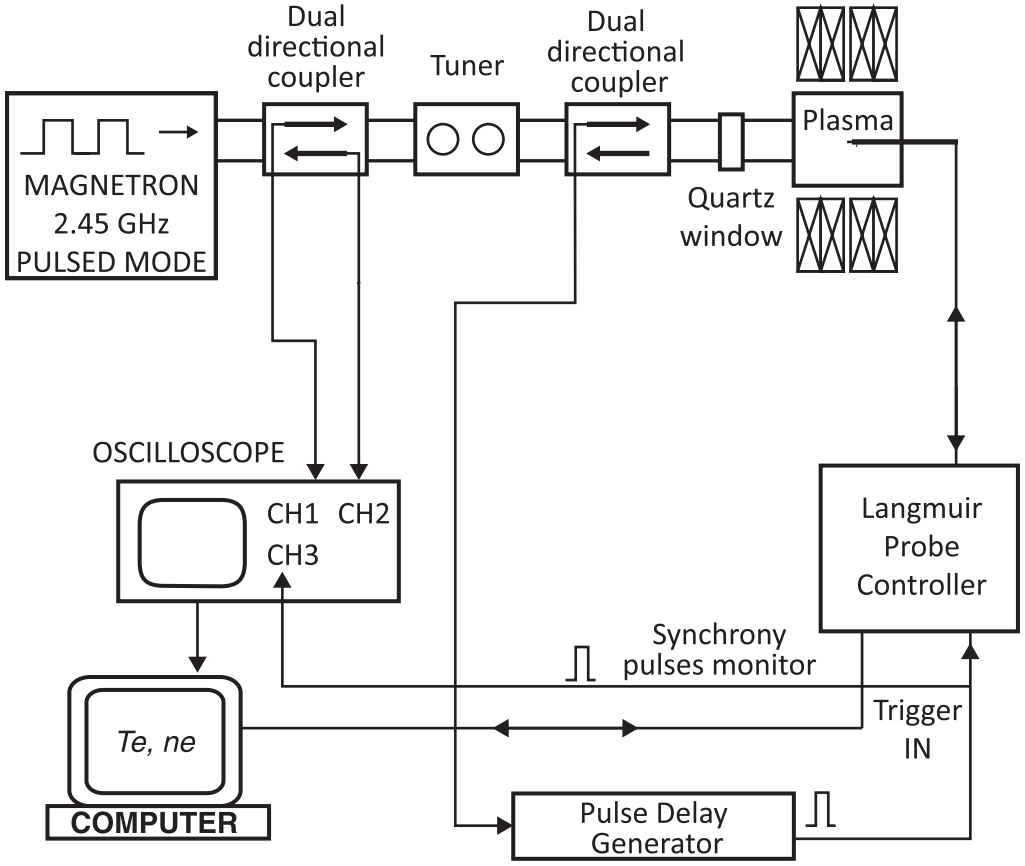

FIG. 6. Experimental arrangement scheme for time resolved density and temperature measurements during decay. Resolution is 200 ns.

potential is null, $I_i(V_p) = 0$, and I_{es} is calculated as the value of the current at the plasma voltage, ergo $I_{es} = I(V_p)$ can be assumed obtaining I_{es} directly from the I-V curve. Theses two calculation branches produce two possible values of electron densities, n_{e1} and n_{e2}, from Eq. (3) with $T_{e,1}$.

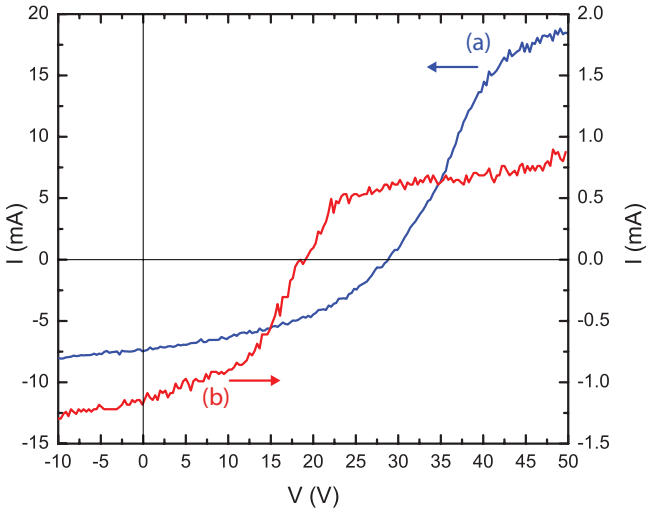

FIG. 7. Langmuir probe I-V curves obtained during the experiments. Curve (a): Typical case during the steady-state plasma condition (100 μs before incoming microwave pulse is off). Curve (b): Typical case corresponding to the decay stage interval of time.

B. Slope of a linear fitting in a current logarithm-voltage representation

This method estimates the electron temperature ($T_{e,2}$) on the basis of the exponential dependence of the electron current with the probe polarization voltage for $V \leq V_p$, i.e.,

$$I_e(V) = I_{es}\, exp\left[\frac{-e(V_p - V)}{kT_e}\right], \tag{4}$$

where T_e is determined by means of the linear fitting slope on a current logarithm-voltage representation of the probe curve. In order to determine the electron density, it is necessary to obtain V_p. At this point, it is important to take into account that V_p can be calculated by using two techniques. The first one is to calculate it as the maximum value of the first I-V derivative like in previous method, and the second one is by the crossing point of two linear fittings in a current logarithm-voltage representation: the one is used to find T_e and another one for fitting the $V > Vp$ branch of the curve. Such values of V_p are usually close. Electron density is calculated by Eq. (3) and the approximations on the ion current have to be made again with two alternatives: linear or parabolic, as is described in the previous method. These calculation branches give two values of density for each plasma potential estimation with finally four more values of electron density n_{e3}, n_{e4}, n_{e5}, and n_{e6}.

A comparison of temperatures and electron densities obtained by the described two methods is shown in Figs. 8 and 9, respectively, under the following experimental conditions:

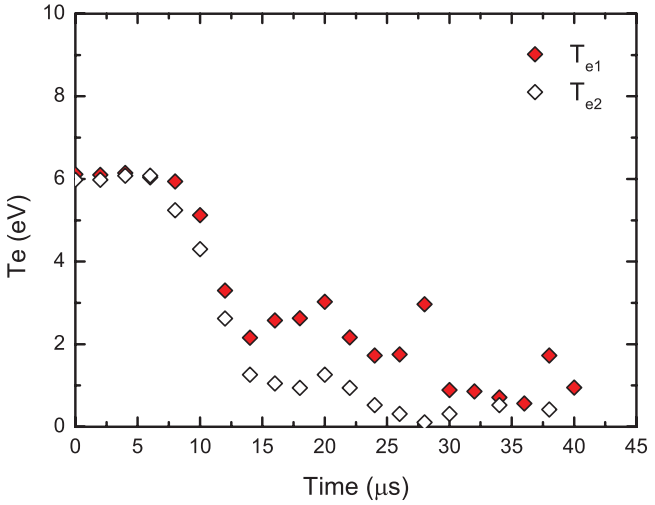

FIG. 8. A comparison of the electron temperatures obtained during the decay process calculated by the two methods described. T_{e1} is estimated by difference of plasma and floating potential. T_{e2} is estimated by measuring the slope in a semilog I-V curve. The error bar in temperature measurement is estimated below 10%, reaching 1 eV at high values during steady state and 0.25 eV during the decay transient.

incoming peak power of 1500 W, pulsed frequency of 100 Hz, duty cycle of 10%, hydrogen pressure 3.8×10^{-3} mbar, and ECR symmetric magnetic profile corresponding with curve (b) and magnetic map (b) of Figs. 2 and 3, respectively. These results are an example of temperature and density evolution obtained during the decay process in order to see how the results depend on the method employed. Note that results keep the shape of the evolution in a relative narrow band of values. This characteristic and its reproducibility suggest that the estimations of plasma parameters can be taken with a reasonable reliability. The error bar in temperature measurement is estimated below 10%, reaching 1 eV at high values during steady state and 0.25 eV during the decay transient. Accuracy in electron density is estimated about 1×10^{16} m^{-3}. In Sec. VI,

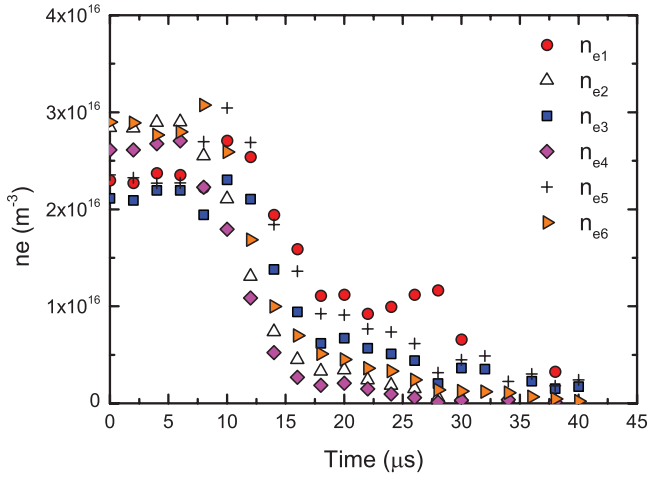

FIG. 9. A comparison of densities values calculated for the decay process. Densities n_{e1} and n_{e2} were obtained by difference of floating potential and plasma potential with linear and parabolic fittings on ion current branch. Densities n_{e3}, n_{e4}, n_{e5}, and n_{e6} were obtained by the slope of $\log(I) - V$ curve for two plasma potentials with both linear and parabolic fittings in each case. Accuracy in electron density is estimated about 1×10^{16} m^{-3}.

TABLE I. Parameters used during the experiments.

Parameter	Values
Magnetic field profile	(a) and (b) of Figs. 2 and 3
Hydrogen pressure (mbar)	3.8 and 6.2×10^{-3}
Peak MW power (W)	300–1500
Duty cycle (%)	10–90
Magnetron pulse frequency (Hz)	100

we present our results on the basis of calculation made using the method of this section with a Laframboise's ion current fitting.

VI. RESULTS

Time resolved electron density and temperature evolution measurements have been conducted simultaneously with the incoming and reflected microwave power signals measurements in our plasma generator. Table I shows the range of parameters where experiments have been conducted. Figure 10 shows two sequences with constant hydrogen pressure of 3.8×10^{-3} mbar at powers between 300 W and 1500 W. The column $B = ECR$ corresponds with resonance magnetic field distribution of Figs. 2(b) and 3(b), and the column $B > ECR$ corresponds to data obtained with the off-resonance magnetic field distribution of Figs. 2(a) and 3(a). Four curves are shown for each magnetic field profile and powers: (a) is the incoming power represented by a dotted line, (b) is the reflected power with a solid line, (c) is the electron temperature with triangular points, and (d) is the electron density with circular empty points. Curves (a) and (b) are in arbitrary units, but (b) is ten times amplified with respect to (a) in order to see the structure of reflected power. In general terms, the plasma coupling shows a better behavior for the off-resonance case of $B > ECR$ where the level of reflected power is initially lower, however, in the resonance case of $B = ECR$, the coupling improves for higher incoming power. Note that for both cases, a pulse of reflected power appears immediately after incoming power starts its decay showing a peak during the final part. After this, an unexpected second pulse or shoulder is observed while the incoming power is practically negligible. For the resonance case of $B = ECR$ the initial value of reflected power at the instant where the incoming power starts its decay is higher. Note for this case that reflected power drops during the beginning of the incoming power decay, but it rebounds showing the first narrow peak mentioned before. A second pulse or shoulder is again recorded during the stage of negligible incoming power. On the other hand, temperature evolution starts at typical values of 8–12 eV corresponding to the steady state of the plasma during the flat top of power pulses. When the incoming power comes down starting its decay process, temperature initially follows the decay but it shows a rebound or peak in coincidence with the second pulse of the reflected power signal just described. Note that temperature decay process follows closely to reflected power signal showing a decay three times longer than incoming power decay time. By contrast, the plasma density evolution shows a more expected

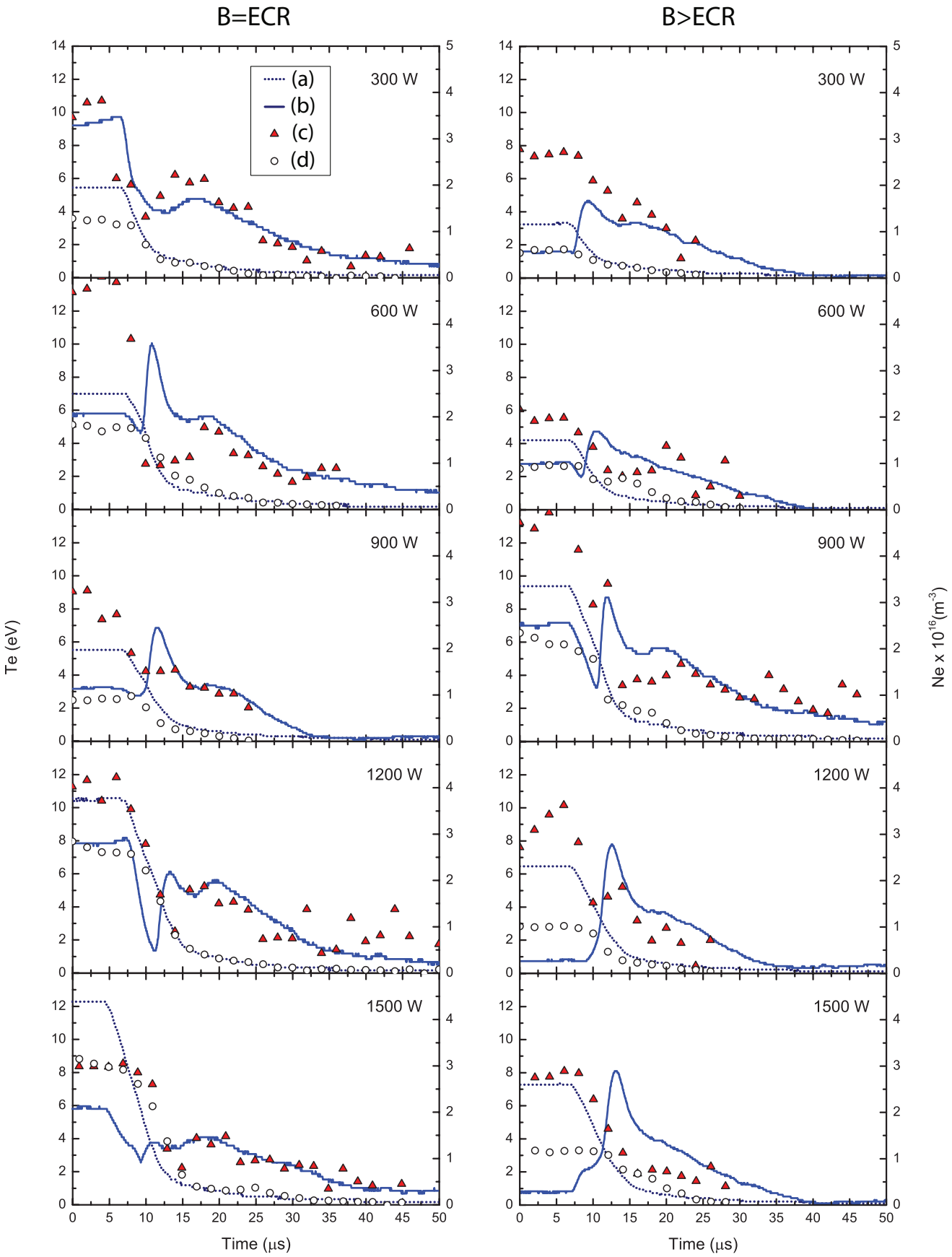

FIG. 10. Evolution of plasma parameters and the incoming and reflected power signals for low pressure (3.8×10^{-3} mbar) and for the two magnetic field profiles used in the experiments: (a) incoming power from magnetron in a.u., (b) reflected power from plasma in a.u. ten times amplified with respect to incoming power, (c) electron temperature, and (d) electron density. The error bar in temperature measurement is estimated below 10% and the accuracy in electron density is estimated about 1×10^{16} m^{-3}.

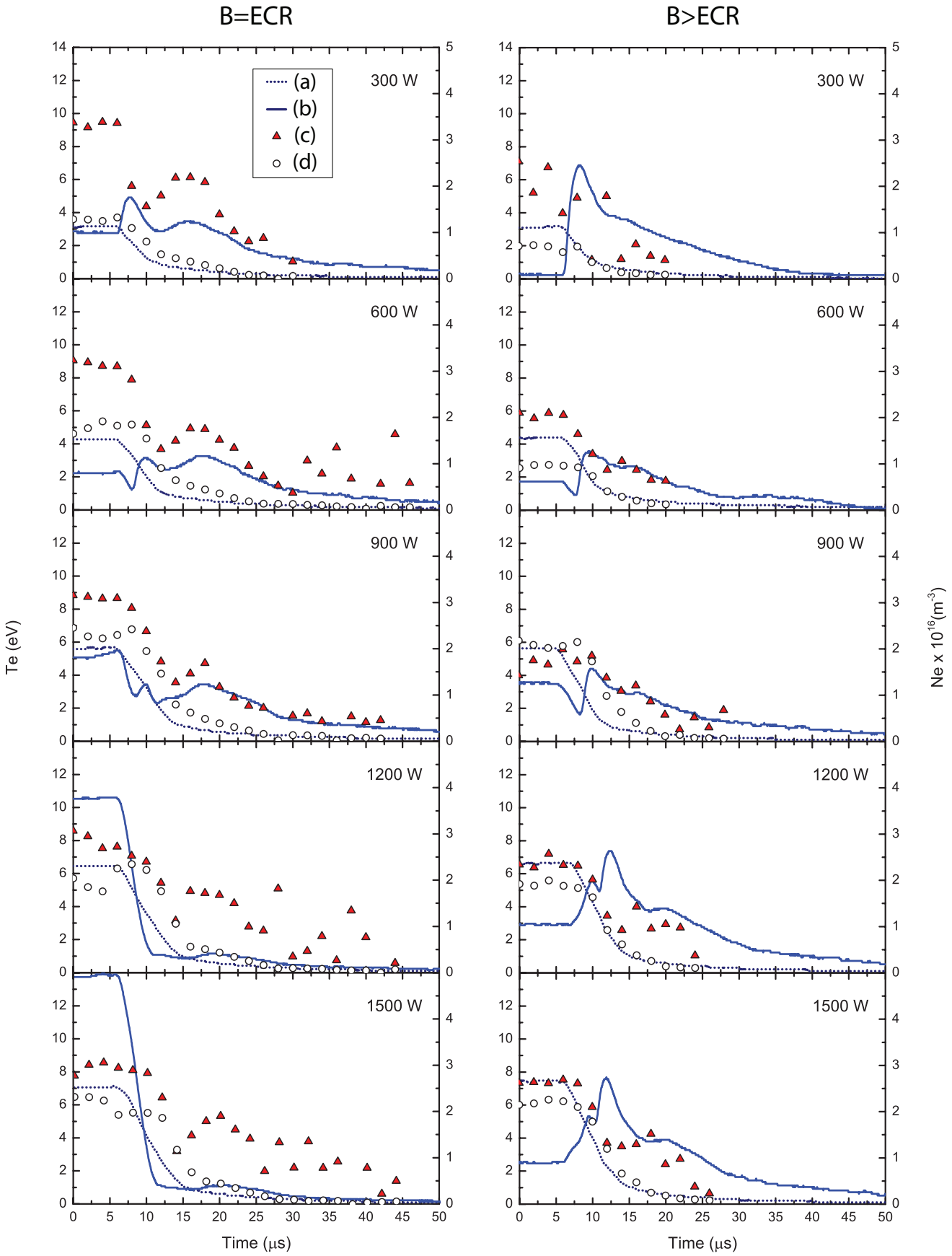

FIG. 11. Evolution of plasma parameters, incoming and reflected powers for higher pressure (6.2×10^{-3} mbar) and the two magnetic field profiles used in the experiments: (a) incoming power from magnetron in a.u., (b) reflected power from plasma in a.u., but ten times amplified with respect to incoming power, (c) electron temperature, and (d) electron density. The error bar in temperature measurement is estimated below 10% and the accuracy in electron density is estimated about 1×10^{16} m^{-3}.

behavior following closely the incoming power signal decay process without an extended decay time.

Figure 11 shows the sequences obtained with a constant hydrogen pressure of 6.2×10^{-3} mbar and powers between 300 W and 1500 W. The column $B = ECR$ corresponds with Figs. 2(b) and 3(b) and the column $B > ECR$ corresponds to data obtained with the magnetic field distribution of Figs. 2(a) and 3(a). The arrangement of graphics follows the same pattern as in Fig. 10 with the same symbols and line styles to facilitate comparisons. For this higher pressure, the plasma coupling is better for the off-resonance case $B > ECR$ as can be seen especially for low incoming powers. The structure of two pulses in the reflected power described previously for lower pressures appears here more notoriously for the cases of $B > ECR$ and for incoming power lower than 900 W at resonance case of $B = ECR$. The temperature rebound is more visible for this higher pressure case generally in coincidence with the second shoulder in the incoming power signal. A notable increment of the decay times for reflected power and temperature is also recorded reaching values of 40 μs, while the density behavior keeps a close tracing of incoming power decay as in previous all cases showing no practical influence from the structure found in the plasma microwave reflected power emission. No significant changes have been observed by modifying the duty cycle in all the magnitudes measured.

VII. DISCUSSION AND CONCLUSION

Plasma temperature and density evolution measurements have been conducted during decay process in our 2.45 GHz hydrogen plasma generator T.I.P.S. Two hydrogen working pressures at two different magnetic field profiles have been studied for a range between 300 W and 1500 W of peak incoming microwave power. Figures 10 and 11 show typical records where the evolution of plasma density and temperature with the incoming and reflected microwave power as temporal reference can be seen. A remarkable structure is observed on the reflected power signal once the incoming power is off. This power is emitted by the plasma without any incoming energy and can be associated to 2.45 GHz plasma decay emission. Also remarkable is the the fact that the emission is recorded at such frequency where the bidirectional coupler sensors sensitivity is centered. This strongly suggests that molecular vibrational decay processes may play an important role in the energy transfer chain during decay. Such structure has been observed during the range of our experiments with a very high reproducibility. The first pulse has a duration of typical 5 μs and it is normally higher than second one which has a typical duration of 15 μs. It is interesting to remark that while the first pulse takes place during the last part of the incoming microwave power decay, the second one is produced while such power is negligible. Simultaneously, electron temperature evolution shows an interesting rebound in coincidence with the second pulse of the plasma reflected microwave emission. By contrast, density evolution always keeps a close tracing of the incoming microwave power decay with no structures and without the extended decay time shown by temperature. Experiments with several duty cycles from 10% to 90% have not reported any significant difference. However, when the coupling ratio between incoming and reflected power before the decay is improved, the structure on reflected power emission is more noticeable as well as the temperature peaks show slightly an incrementing tendency. Increments of the decay times for reflected power and temperature evolution are also recorded reaching values of 40 μs when hydrogen pressure is also increased. Temperature peaks show a relative increment at $B = ECR$ magnetic field distribution, while for the $B > ECR$ profile structure shows shorter decay times reaching half values of the ECR case. This behavior is recorded for both studied pressures. All data suggest that the main factor that produces some influence on the general behavior is the incoming, and reflected power ratio from the plasma. This fact strongly suggests that final values of the plasma parameters before the shutdown and the interplay with the incoming microwave power during this kind of *decoupling* process may be determinant for the ulterior dynamics of the plasma parameters evolution.

On the other hand, It is a remarkable fact that temperature structure shows a behavior virtually independent of the set of parameters studied. This may suggest some connection with similar behaviors reported in bremsstrahlung emission for ECRIS working at higher microwave frequencies that are related with instabilities during afterglow phenomenon.[4,21,22] Temperature rebounds could be explained in terms of energy distribution in a collection of particles (electrons) whose population is descending as well as density drops. Once the incoming power starts falling, it is reasonable to suppose a decrease of plasma density from the steady state value due to the ionization rate drop. This gradual decrease of density is shown by our measurements in Figs. 10 and 11. Such behavior can produce some relative increment in the reflected power because coupling became worst and worst until reaching a situation where the fast lost of electrons during this stage produces a deep change in the EEDF. On the other hand, the influence of plasma parameters evolution should be determining on the plasma microwave emission once the incoming power is off. A further work on calculations of EEDFs on the basis of experimental probe data is in the aim of our group to explain these observations for the near future.

ACKNOWLEDGMENTS

This work was supported for ESS Bilbao Consortium. The authors want to express their gratitude to F. J. Bermejo for his continuous support and O. Tarvainen for his always useful discussions and suggestions.

[1]G. Melin, F. Bourg, P. Briand, J. Debernardi, M. Delaunay, R. Geller, B. Jacquot, P. Ludwig, T. N'Guyen, L. Pin, M. Pontonnier, J. Rocco, and F. Zadworny, Rev. Sci. Instrum. **61**, 236 (1990).
[2]P. Sortais, J. L. Bouly, J. Curdy, T. Lamy, P. Sole, T. Thuillier, J. L. Vieux-Rochaz, and D. Voulot, Rev. Sci. Instrum. **75**, 1610 (2004).
[3]H. Bäcker, J. W. Bradley, P. J. Kelly, and R. D. Arnell, J. Phys. D: Appl. Phys. **34**, 2709 (2001).
[4]O. Tarvainen, T. Ropponen, V. Toivanen, T. Kalvas, J. Ärje, and H. Koivisto, Plasma Sources Sci. Technol. **19**, 045027 (2010).
[5]N. Britun, T. Godfroid, S. Konstantinidis, and R. Snyders, Appl. Phys. Lett. **98**, 141502 (2011).

[6]I. Izotov, D. Mansfeld, V. Skalyga, V. Zorin, T. Grahn, T. Kalvas, H. Koivisto, J. Kompula, P. Peura, O. Tarvainen, and V. Toivainen, Phys. Plasmas **19**, 122501 (2012).
[7]O. D. Cortázar, A. Megía-Macías, and A. Vizcaíno-de Julián, Rev. Sci. Instrum. **83**, 103302 (2012).
[8]O. D. Cortázar, A. Megía-Macías, and A. Vizcaíno-de Julián, IEEE Trans. Plasma Sci. **40**, 3409 (2012).
[9]O. D. Cortázar, A. Megía-Macías, and A. Vizcaíno-de Julián, in *Proceedings of ECRIS 2012*, Sidney, Australia, 2012 (JACoW.org, in press).
[10]O. D. Cortázar, J. Komppula, O. Tarvainen, A. Megía-Macías, A. Vizcaíno-de Julián, and H. Koivisto, Plasma Sources Sci. Technol. **22**, 015026 (2013).
[11]A. Rousseau, E. Teboul, N. Lang, M. Hannemann, and J. Röpcke, J. Appl. Phys. **92**, 3463 (2002).
[12]F. Chen, Plasma Sources Sci. Technol. **18**, 035012 (2009).
[13]R. L. Merlino, Am. J. Phys. **75**, 1078 (2007).
[14]F. F. Chen, *Plasma Diagnostics Techniques*, edited by R. H. Huddlestone and S. L. Leonard (Academic Press, New York, 1965).
[15]J. Jauberteau and I. Jauberteau, Rev. Sci. Instrum. **78**, 043501 (2007).
[16]V. Godyak and V. Demidov, J. Phys. D: Appl. Phys. **44**, 233001 (2011).
[17]M. Lieberman and A. Lichtemberg, *Principles of Plasma Discharges and Material Processing* (Wiley, 1994), p. 189.
[18]I. Saudit and F. Chen, Plasma Sources Sci. Technol. **3**, 162 (1994).
[19]F. Chen, J. Evans, and D. Arnush, Phys. Plasmas **9**, 1449 (2002).
[20]M. Tuszewski and J. A. Tobin, Plasma Sources Sci. Technol. **5**, 640 (1996).
[21]K. Tinschert, R. Ianucci, J. Bossler, and R. Lang, Rev. Sci. Instrum. **75**, 1407 (2004).
[22]R. Geller, *Electron Cyclotron Resonance Ion Sources and ECR Plasmas* (Institute of Physics Publishing, Bristol, UK, 1996).